Structural and Thermodynamic Features of Spiroiminodihydantoin Damaged DNA Duplexes†

Lei Jia,‡ Vladimir Shafirovich,‡ Robert Shapiro,‡ Nicholas E. Geacintov,‡ and Suse Broyde*,‡,§

Departments of Chemistry and Biology, New York University, New York, New York 10003

Received April 28, 2005; Revised Manuscript Received July 20, 2005

ABSTRACT: Oxidation of guanine or 8-oxo-7,8-dihydroguanine can produce spiroiminodihydantoin (Sp) *R* and *S* stereoisomers. Both in vitro and in vivo experiments have shown that the Sp stereoisomers are highly mutagenic, causing G → C and G → T transversion mutations. Therefore, they are of interest as potential endogenous cancer causing lesions. However, their structural properties in DNA duplexes remain to be elucidated. We have employed computational methods to study the Sp lesions in 11-mer DNA duplexes with A, C, G, and T partners. Molecular dynamics simulations have been carried out to obtain ensembles of structures, and the trajectories were employed to analyze the structures and compute free energies. The structural and thermodynamic analyses reveal that the Sp stereoisomers energetically favor positioning in the B-DNA major groove, with minor groove conformers also low energy in some cases, depending on the partner base. The *R* and *S* stereoisomers adopt opposite orientations with respect to the 5′ to 3′ direction of the modified strand. Both *syn* and *anti* glycosidic bond conformations are energetically feasible, with partner base and stereochemistry determining the preference. The lesions adversely impact base stacking and Watson−Crick hydrogen bonding interactions in the duplex, and cause groove widening. The chemical nature of the partner base determines specific hydrogen bonding and stacking properties of the damaged duplexes. The structural characteristics may relate to observed mutagenic properties of the Sp stereoisomers, including possible stereoisomer-dependent differences.

Reactive oxygen species, present in the cell as a consequence of normal respiration, or produced by ionizing radiation, can attack DNA bases and produce DNA base lesions (*1*−*8*). The most important of these is 8-oxo-7,8-dihydroguanine (8-oxoG)[1] (*9*). Further oxidation can lead to a number of derivatives including cyanuric acid (Ca), oxaluric acid (Oa), oxazolone (Oz), imidazolone (Iz), nitroimidazole (NI), urea (Ua), spiroiminodihydantoin (Sp), guanidinohydantoin (Gh), and iminoallantoin (Ia) (*10*−*14*).

The *R* and *S* spiroiminodihydantoin (Sp) stereoisomers (Figure 1A) result from the direct oxidation of guanine and the further oxidation of 8-oxoG (*15*−*32*). Recently, Sp was detected in Nei-deficient *Escherichia coli* following chromate exposure (*33*). Our previous high level quantum mechanical (QM) geometry optimization studies for these DNA lesions have shown that the Sp *R* and *S* stereoisomers are enantiomers with two rigid and nearly flat five-membered rings essentially perpendicular to one another (Figure 1B) (*34*).

Because of the unique chemical structures of the Sp lesions, their biological functions are of great interest. It has been demonstrated that the Sp lesions block polymerases and cause mutations, both in vitro and in vivo (*35*, *36*). In vitro, primer extension experiments using KF exo⁻ show that Sp can be bypassed by misinserting either adenine or guanine opposite these lesions (*35*). The insertion of adenine is favored over that of guanine, while incorporation of cytosine and thymine opposite Sp is not observed (*35*). Such Sp·A and Sp·G mismatches have been also observed in in vivo studies (*36*). When DNA containing site-specifically positioned Sp lesions is transfected into *E. coli*, DNA polymerases are primarily blocked by both Sp stereoisomers, but rare bypass events produce G → C and G → T transversion mutations. Furthermore, the Sp lesions lead to a higher rate of G → C and G → T transversion mutations than are observed in the case of 8-oxoG (*37*).

Oxidative DNA base damages are repaired by the base excision repair (BER) system (*38*−*40*). An array of BER enzymes have been investigated with respect to their ability to excise the Sp lesions. In vitro studies have shown that Sp lesions opposite guanine and cytosine are removed by all three oxidized base-specific DNA glycosylases of *E. coli* (*41*, *42*): 8-oxoG DNA glycosylase (Fpg or MutM), endonuclease III (Nth), and endonuclease VIII (Nei). MutM preferentially

† This research is supported by NIH Grant CA-75449 to S.B. and NIH Grant ES-11589 to V.S. and N.E.G.

* Corresponding author. Tel: (212) 998-8231. Fax: (212) 995-4015. E-mail: broyde@nyu.edu.

‡ Department of Chemistry.

§ Department of Biology.

[1] Abbreviations: 8-oxoG, 8-oxo-7,8-dihydroguanine; Ca, cyanuric acid; Oa, oxaluric acid; Oz, oxazolone; Iz, imidazolone; NI, nitroimidazole; Ua, urea; Sp, spiroiminodihydantoin; Gh, guanidinohydantoin; Ia, iminoallantoin; QM, quantum mechanics; KF, Klenow fragment; BER, base excision repair; Fpg/MutM, formamidopyrimidine glycosylase; Nth, endonuclease III; Nei, endonuclease VIII; MutY, adenine DNA glycosylase; yOGG, yeast 8-oxoG glycosylase; hOGG, human 8-oxoG glycosylase; NEIL, endonuclease VIII like; MD, molecular dynamics; G, guanine; A, adenine; C, cytosine; T, thymine; RESP, restrained electrostatic potential fitting algorithm; PME, particle mesh Ewald; RMSD, root-mean-square deviations; MM-PBSA, molecular mechanics Poisson−Boltzmann surface area; SASA, solvent accessible surface area.

10.1021/bi050790v CCC: $30.25
Published on Web 09/16/2005

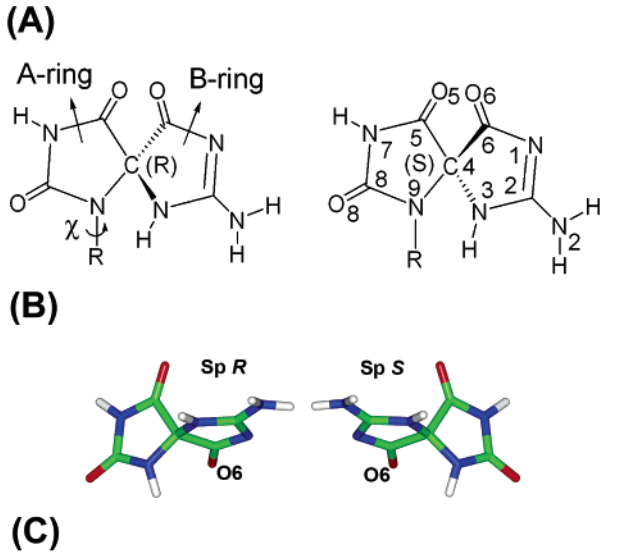

FIGURE 1: (A) Structures of spiroiminodihydantoin *R* and *S* stereoisomers. **R** is deoxyribose. Atom numbers are defined for the *S* stereoisomer. The glycosidic torsion angle χ is O4′(**R**)−C1′(**R**)−N9−C4 (*68*) and is marked on the *R* stereoisomer. (B) Structures of Sp *R* and *S* stereoisomers after QM geometry optimization. (C) Sequences for the molecular dynamics simulations.

excises Sp opposite C, while Nei prefers to remove Sp opposite G, but also excises Sp opposite A. Nth is less active than the other two enzymes. The 8-oxoG·A-specific adenine glycosylase MutY, observed to remove 8-oxoG paired with adenine, cannot remove Sp lesions mispaired with A. Also, MutY significantly inhibits the MutM repair of Sp·C. The functionally related yeast enzymes yOGG1 and yOGG2 also remove Sp, irrespective of the base on the complementary strand, while the human homologue hOGG1 cannot remove Sp in any base-pairing context (*43*). Importantly, two recently identified mammalian glycosylases, NEIL1 and NEIL2, show activity in the repair of Sp lesions. The murine NEIL1 BER enzyme can remove Sp when paired with all four bases. However, NEIL2 has only low activity (*37*).

A knowledge of the structures of Sp-damaged DNA is needed to elucidate their biological functions, but there are, at present, no experimental structures of DNA duplexes with Sp lesions. To delineate how the Sp stereoisomers damage DNA duplexes, we have employed computational methods to study these lesions in 11-mer DNA duplexes with A, C, G, and T opposite Sp. Molecular dynamics (MD) simulations in aqueous solution were carried out to obtain ensembles of structures, and trajectories were employed to analyze the structures and compute free energies. The structural and thermodynamic analyses show that the Sp stereoisomers energetically favor positioning in the B-DNA major groove, with minor groove conformers also low energy in some cases, depending on the partner base. The *R* and *S* stereoisomers adopt opposite orientations with respect to the 5′ to 3′ direction of the modified strand. Both *syn* and *anti* glycosidic bond conformations are feasible, with partner base and stereochemistry determining the preference. Specific hydrogen bonding interactions between the Sp lesions and partner bases can form in some cases; the best interactions are with G in the low energy structures. In addition, the *R* and *S* stereoisomers adopt opposite orientations with respect to the 5′ to 3′ direction of the modified strand. Distortions to the modified duplexes involve a diminished quality of Watson−Crick hydrogen bonding and weakened stacking interactions, as well as a widening of the grooves. These structural properties may play a role in the observed mutagenic properties and repair susceptibilities of the Sp stereoisomers, including the possibility of stereoisomer-dependent differences. If the mutations are produced in genes governing the control of the cell cycle, the initiation of cancer may occur (*44*−*47*).

METHODS

Initial Structures. Our previously obtained quantum mechanically geometry optimized structures (Figure 1B) for the Sp *R* and *S* stereoisomers were employed in the present study. We created initial models for the molecular dynamics simulations in the sequence shown in Figure 1C by replacing an unmodified guanine with the *R*- or *S*-Sp in an energy minimized (*48*) B-DNA of that sequence. In addition, mismatches were created by replacing the Sp partner C with A, G, or T. Both *syn* and *anti* glycosidic bond orientations for Sp lesions, as well as for their partners when these were purines opposite Sp(*anti*) (*49*, *50*), were considered. We did not consider *syn*−*syn* pairing or *syn* pyrimidines since these are rarely observed (*51*). The B-DNA energy minimized values for χ were employed for the *anti* partner structures, while the *syn* structures were obtained by rotation of χ by about 180°, using optimal stacking as the criterion for the actual *syn* χ values. Table S1 (Supporting Information) gives χ values of Sp employed in all starting models. Representative starting structures are shown in Figure S1 (Supporting Information).

Force Field. Computations were carried out with the AMBER 8.0 (*52*) suite of programs, the Cornell et al. force field (*53*), and the PARM99 parameter set (*54*). The force field was parametrized for the Sp *R* and *S* stereoisomers consistent with the rest of the force field. Partial charges for the Sp *R* and *S* stereoisomers were separately obtained as described by Cieplak et al. (*55*); HF calculations with the 6-31G* basis set (*56*) were used to calculate the electrostatic potential using Gaussian98 (*57*), and the restrained electrostatic potential fitting algorithm RESP (*55*, *58*) was employed to fit the charge to each atom center. Partial charges were separately computed for *anti* ($\chi = 240°$) and *syn* ($\chi = 60°$) conformers for each stereoisomer and averaged. New atom types were defined for the Sp moieties. Bond length and angle equilibrium values for the Sp were taken from the QM optimized structures. Bond length and angle force constant parameters not present in the PARM99 parameter set were assigned by analogy with chemically similar atom types already present in the AMBER force field. Because of the unusual Sp structures, test MD simulations revealed that bond angles around the Sp N9 and sugar C1′ deviated markedly from the QM optimized values for Sp and from standard values in the AMBER force field; therefore, modest increases

to bond angle force constants, remaining within AMBER ranges, were made to achieve bond angles near the equilibrium ranges. All of the added force field parameters, atom types, and topology assignments are listed in Tables S2 and S3 (Supporting Information).

Molecular Dynamics Protocol. Details of the MD protocol (*52*, *59*−*65*) are given in the Supporting Information.

Stability of the Molecular Dynamics Simulation. Plots of root-mean-square deviations (RMSD) of the current relative to the starting structure, as a function of time, are shown in Figure S2 (Supporting Information). The structures generally fluctuate stably after 1.5 ns, and our further analyses employed the 1.5−3.0 ns time frame.

Structural Analyses. Snapshots of the DNA structures during the simulation and the average structures, with solvent and counterions stripped away, were obtained with the PTRAJ module of the AMBER 8.0 suite. PTRAJ was also employed to obtain time-dependence of the RMSD, the glycosidic torsion angle χ and the sugar pucker **P** (*66*) of the Sp *R* and *S* residues, and the corresponding dG residue in the unmodified control. Hydrogen bonding analyses were carried out with the CARNAL module of the AMBER 7.0 suite (*67*). In addition, we employed a hydrogen bond quality index (*48*), I_H, to quantitatively assess the deviation from ideal Watson−Crick hydrogen bonding distances and angles for 5′ and 3′ neighboring base pairs of Sp:

$$I_H = \sum_{D-H\cdots A} [(d_{DA} - d^0_{DA})^2 + (1 + \cos\gamma)^2]$$

where d_{DA} is the instantaneous donor−acceptor distance, d^0_{DA} is an ideal donor−acceptor distance (*68*) (N4 (C) to O6 (G) is 2.91 Å, N1 (G) to N3 (C) is 2.95 Å, and N2 (G) to O2 (C) is 2.86 Å), and γ is the instantaneous D−H···A bond angle with ideal value of 180°. The summation is over the three Watson−Crick hydrogen bonds in a G·C base pair and then over the selected trajectory window. I_H adopts a value of 0 when ideal Watson−Crick hydrogen bonding is maintained. The DNA groove width and backbone torsions were analyzed with MD Toolchest (*69*, *70*). The bend angle of the duplex was analyzed with the program CURVES (*71*), employing the "PP" option, which yields a bend angle measured between the vectors composed of the first two and last two reference points defining the axis. The first and last base pair were removed prior to this analysis. In addition, we removed the Sp and its partner when the partner was *syn* since CURVES could not recognize these moieties. The computed bend angles were thus based on global helix axes determined by the four base pairs surrounding the lesion in each direction. The stacking interactions were evaluated by computing the van der Waals interaction between adjacent base pairs, including the Sp lesion-containing pair, with the program ANAL from the AMBER 7.0 suite (*67*).

Free Energy Analyses. The molecular mechanics Poisson−Boltzmann surface area (MM-PBSA) method which has been described in detail (*72*−*77*) was employed to perform the free energy analyses. In brief, the free energy (G_{tot}) was computed from the molecular mechanical energies (E_{MM}), the solvation free energy ($G_{solvation}$), and the solute entropic contributions to the free energy ($G_{tot} = E_{MM} + G_{solvation} - TS$) (*78*, *79*). The molecular mechanical energies (E_{MM}) were calculated from internal energies (E_{int}) stemming from deviations of the bonds (E_{bonds}), angles (E_{angles}), and dihedral angles ($E_{dihedrals}$) from their equilibrium values, the van der Waals energies (E_{vdW}), and electrostatic energies ($E_{electrostatic}$). The solvation free energies ($G_{solvation}$) were estimated from the electrostatic solvation energies (G_{PB}) calculated using the DelPhi program (*80*) and the nonpolar solvation energy ($G_{nonpolar}$); the latter was approximated as $G_{nonpolar} = \gamma S_A + b$ ($\gamma = 0.00542$ kcal/Å^2, $b = 0.92$ kcal/mol) (*81*), where S_A is the solvent accessible surface area (SASA) (*82*) computed by Sanner's algorithm in the MSMS program (*83*). The solute entropic contributions to the free energies were approximated with normal mode calculations (*84*). Details of the protocol (*52*−*54*, *82*, *85*) are given in the Supporting Information.

INSIGHT II from Accelrys, Inc. was employed for visualization and model building. Computations were carried out on our own cluster of Silicon Graphic Origin and Altix supercomputers and Octane workstations, as well as at the NYU Information Technology Services Origin300 supercomputer.

RESULTS

The goal of our work was to investigate structures of the Sp *R* and *S* stereoisomers in DNA duplexes in solution. We carried out 3 ns molecular dynamics simulations, to obtain ensembles of structures. Each Sp stereoisomer was investigated in four 11-mer B-DNA duplexes in which the partner base opposite the Sp was A, C, G, or T. In addition we investigated an unmodified control duplex containing a normal G·C pair in place of the damaged site. We considered both *syn* and *anti* glycosidic bond orientations for the Sp modifications, as well as for their partners when these were purines opposite Sp(*anti*) (*49*, *50*). *Syn*−*syn* pairings are extremely uncommon, and pyrimidines adopt the *syn* conformation only very rarely (*51*). Detailed analyses of the MD generated ensemble were performed to delineate the structural and thermodynamic features of these lesion-containing DNA duplexes.

Structural Analyses

Syn Sp places the Lesion in the Major Groove. We first focus on the structures with the Sp glycosidic bond orientation in the *syn* domain. Here we observe from Figure 2 that the Sp perpendicular rings are located in the DNA major groove. In the case of the *R* stereoisomer the distal B-ring of the propeller-like structure is oriented so that it is directed toward the 3′ end of the modified strand with the O6 atom 3′-directed. By contrast, in the *S* stereoisomer, the B-ring and its O6 atom is 5′-directed. The A-ring is inserted into the helix in each case. Detailed structural analyses show general enlargement of the major groove, to accommodate the Sp rings, as well as perturbations to hydrogen bonding and stacking (Figure 3 and Figures S4−S7 and S10 (Supporting Information)).

We monitored bend angles as a function of time and found that the trajectory-averaged bend angles usually differed only little from the unmodified control when the Sp glycosidic bond orientation is *syn* (Figures S4−S7). The largest difference is only about 5°.

Analyses of the sugar pucker pseudorotation **P** show that the unmodified control remained in the normal B-DNA C2′-endo conformation (**P** in the southern region of the pseu-

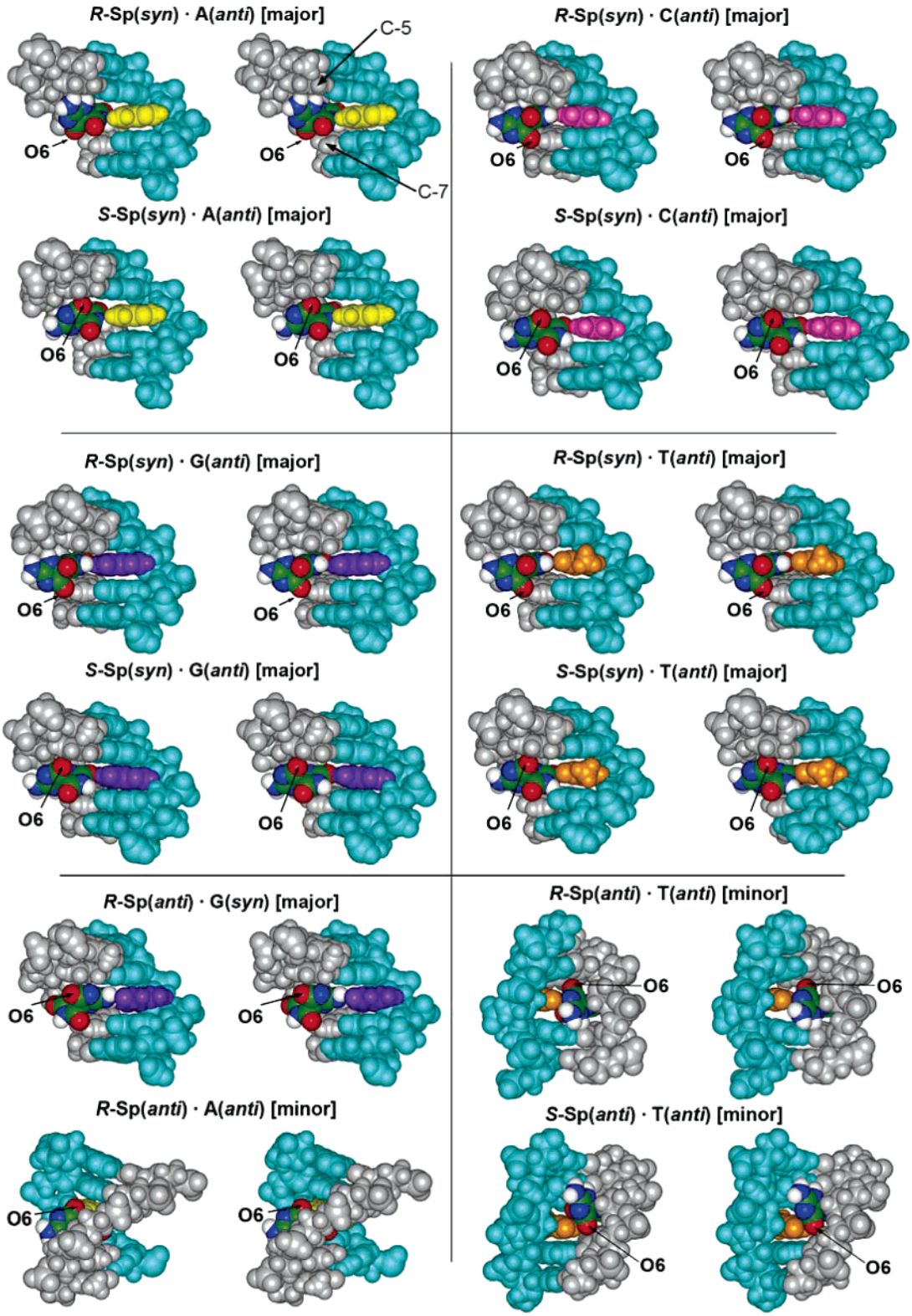

FIGURE 2: Stereoviews of the central 5-mer of the Sp trajectory-average duplex structures in CPK models. The low energy structures of Table 1 are shown, except *R*-Sp(*syn*)·T(*anti*). The Sp stereoisomers are colored by atom. The Sp base partners are colored as yellow (A), pink (C), purple (G), and orange (T). The oppositely oriented O6 atoms are marked. The Sp adjacent bases C5 and C7 are also marked in gray. Sp conformational families are designated. All stereo figures are prepared for viewing with a stereoviewer.

dorotation cycle at around 180°) (*66*). In the case of the Sp modified duplexes the sugar pucker is more flexible, generally sampling both C2′-endo and C3′-endo conformations (**P** in the northern region of the pseudorotation cycle at around 0°). In addition, the Sp stereoisomers are much more prone to sample the less common O4′-endo sugar conformation (**P** in the eastern region of the pseudorotation cycle at around 90°) than the unmodified duplex (Figures S4−S7).

The glycosidic bond χ remains in the *syn* domain in all the modified duplexes, while it retains its normal B-DNA value in the *anti* ($\chi \sim 240°$) domain in the unmodified duplex. However, for the *R* stereoisomer, two regions of the

Table 1: Relative Free Energies (kcal/mol)[a]

	Sp(*anti*)·X(*anti*)	Sp(*syn*)·X(*anti*)	Sp(*anti*)·X(*syn*)
R-Sp·A	0 (minor)	1.0 (major)	6.7 (minor)
S-Sp·A	7.9 (major)	0 (major)	4.8 (major)
R-Sp·C	4.5 (major)	0 (major)	
S-Sp·C	10.0 (intercalated)	0 (major)	
R-Sp·G	3.8 (minor)	0.2 (major)	0 (major)
S-Sp·G	6.9 (minor)	0 (major)	9.8 (intercalated)
R-Sp·T	0 (minor)	6.4 (major)	
S-Sp·T	0 (minor)	0.2 (major)	

[a] The lowest energy structure for each sequence and stereoisomer is 0 kcal/mol. Major, minor, and intercalated indicate Sp location is in the major or minor groove, or intercalated into DNA duplex.

overall *syn* domain are sampled, one at ~60° and the second at ~100°, except for the case of Sp paired with A, where only the ~30° region is found (Figures S4−S7). The O4′-endo sugar pucker is correlated with the *syn* χ at ~30° when A is the partner, and contributes to the stabilization of a hydrogen bond between N7H7 of the Sp and N1 of A, as detailed below.

Specific hydrogen bonding features of the Sp lesions with their partner bases are shown in Figures 3 and S10. We observe that one normal hydrogen bond is formed when C or A is opposite Sp for both stereoisomers, and when T is opposite the *S* Sp. With G opposite the Sp, one bifurcated hydrogen bond is found, with O8 of the Sp as the acceptor and the N1H1 and N2H2 of the G as the donors. With T opposite *R* Sp, two hydrogen bonds are formed. Other hydrogen bonding interactions involving the Sp are shown in Table S5 (Supporting Information). Specifically, we note that Sp can also form hydrogen bonds to neighboring bases on the modified and/or partner strands. More such hydrogen bonding interactions occur when G and T are paired with either *R*- or *S*-Sp than when the opposite base is A or C. In addition, we see that the *R* stereoisomer forms more and better hydrogen bonds, regardless of the partner base, than the *S* stereoisomer.

In addition, we analyzed the Watson−Crick hydrogen bonding properties of the base pairs adjacent to the lesions. We find that Watson−Crick pairing is generally present most of the time in the adjacent base pairs (Figure S11 (Supporting Information)). However, the quality of hydrogen bonding is adversely impacted. To evaluate this effect, we computed the Watson−Crick hydrogen bond quality index (see Methods) for the neighboring pairs C5·G18 and C7·G16 (Figure 4). Our results show that, for the *S* stereoisomer, the Sp 3′-neighboring C7·G16 pair is more disturbed than the 5′-neighboring C5·G18 pair; however, for the *R* stereoisomer (except when A is the partner), the Sp 5′-neighboring C5·G18 pair is distorted. Furthermore, the disturbance is greater in the 3′ direction for the *S* stereoisomer than the 5′ direction for the *R* stereoisomer. The stereochemistry of the *R* and *S* stereoisomers plays the fundamental role in this directional perturbation of Watson−Crick pairing. Specifically, the orientation of the Sp O6 atom is critical. In the *R* stereoisomer, it is 3′-directed in the groove, in a less crowded position of the right-hand-twisted double helix. However, in the *S* stereoisomer, the O6 is 5′-directed and in a more crowded situation (Figure 2), causing this stereochemical effect. In the special case of partner A, hydrogen bonds form between A and *R*-Sp (Figure 3), which orient the Sp to allow an additional hydrogen bond between N3H3 of Sp and N3 of C5 (Table S5); this has the effect of distorting the

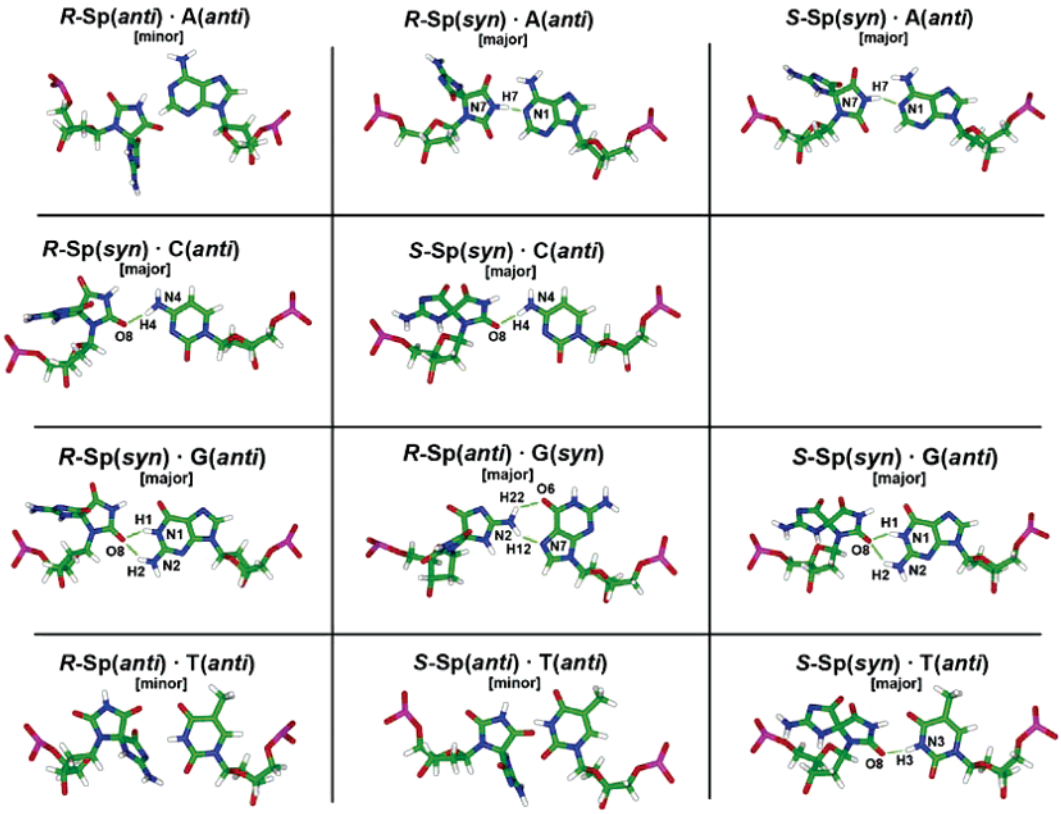

FIGURE 3: Hydrogen bonds (green lines) between Sp and partner base. The low energy structures of Table 1 are shown. The base pairs are obtained from the trajectory average structures of the selected simulation window. Hydrogen bonds shown have occupancy greater than 50%.

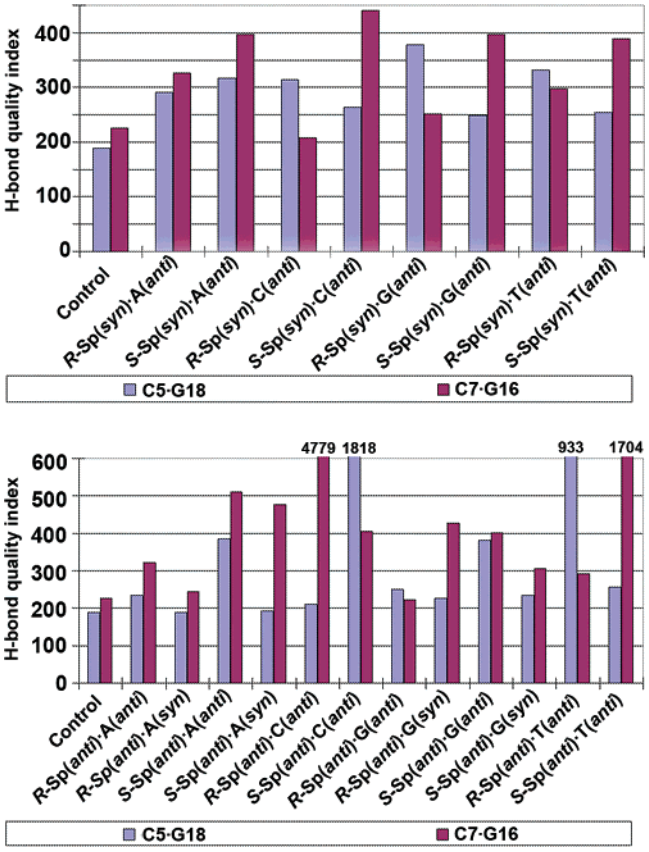

FIGURE 4: Trajectory summed hydrogen bond quality index for the 5′ (C5·G18) and 3′ (C7·G16) Sp neighboring Watson−Crick base pairs. The values for C5·G18 in *S*-Sp(*anti*)·C(*anti*), C7·G16 in *R*-Sp(*anti*)·C(*anti*), C5·G18 in *R*-Sp(*anti*)·T(*anti*), and C7·G16 in *S*-Sp(*anti*)·T(*anti*) are not shown to full scale; their values are given at the top of the bar.

C7·G16 pair, because the Sp A-ring is directed toward this pair (Figure 2). As a consequence, the *R*-Sp A-ring distorts the adjacent bases. However, the Sp B-ring becomes particularly well positioned in the major groove, nicely following the twist of the groove (Figure 2). Thus, the Sp A-ring causes less DNA distortion than when C, G, and T are partners.

Anti Sp with the Lesion in the Major or Minor Groove, or Intercalated. When the Sp residue is *anti*, an obvious position for the perpendicular Sp rings is insertion into the duplex between adjacent base pairs, and *anti* starting models for the MD simulations adopted intercalated structures. Our simulations show that this structural type of family remained stable only in the case of the Sp *S* stereoisomer when paired with C(*anti*), and when paired with G(*syn*) (Figure S9 (Supporting Information)). In other cases the Sp rearranged during the MD to reside in the major or minor groove. The major groove conformers are observed in the case of the *R* stereoisomer when paired with C(*anti*) and G(*syn*), and the Sp *S* stereoisomer when paired with A(*anti*) and A(*syn*) (Figures 2 and S9). The minor groove conformers are noted for Sp *R* and *S* stereoisomers paired with G(*anti*), T(*anti*), and for the *R*-Sp stereoisomer paired with A(*anti*) and A(*syn*) (Figures 2 and S9). Opposite orientations of the Sp B-rings are found in the *R* and *S* stereoisomers in both the major and minor groove *anti* conformations. Specifically, the Sp O6 atom is 5′-directed for the *R* stereoisomer and 3′-directed for the *S* stereoisomer (Figures 2 and S9), opposite to their orientations for the corresponding *syn* structures (Figure 2). No intercalated conformations remained stable for the *R* stereoisomer.

The intercalated structures are severely distorting. Accommodation of the Sp perpendicular rings within the duplex requires local stretching, unwinding, major groove enlargement with concomitant minor groove narrowing, and serious distortion to either or both adjacent base pairs (Figures S4−S8 (Supporting Information)). Base stacking interactions are interrupted, and there is no stacking involving the Sp rings. No hydrogen bonding between Sp and partner base is found in this family. However, the Sp moiety is held in the intercalated position by hydrogen bonds to the partner strand: N3H3 of Sp to N3 of G18 in the case of *S*-Sp paired with C(*anti*), and N2H2 of Sp to O4′ of G18 and N3H3 of Sp to N3 of G18 in the case of *S*-Sp paired with G(*syn*). In addition, a high degree of flexible bending is found in the *S*-Sp stereoisomer opposite C(*anti*), but not opposite G(*syn*). The extent of bending in the latter resembles that in the unmodified duplex (Figure S8). Thermodynamic analyses, detailed below, show that this structural family is energetically disfavored.

The major groove conformations are less distorting. However, the Sp B-ring is still accommodated within the helix. This leads to major groove opening and concomitant minor groove narrowing (Figures S4−S8). In addition, the neighboring Watson−Crick base pairs are perturbed, with the C7·G16 pair more perturbed than C5·G18, regardless of the stereoisomer or partner base (Figure 4). There is no stacking involving the Sp rings with the adjacent bases. The Sp B-ring of the *R* stereoisomer is directed toward the C5 position, and the perpendicular A-ring disturbs the C7·G16 base pair. However, the Sp B-ring of the *S* stereoisomer is directed toward the C7 position and disturbs the C7·G16 base pair (Figures 2 and S9). In this conformational family, hydrogen bonding between Sp and its partner base is found in the following cases: *S*-Sp·A(*anti*) pair (N2H2 of Sp to N1 of A) and *R*-Sp·G(*syn*) pair (N2H2 of Sp to O6 of G, and N2H2 of Sp to N7 of G) (Figures 3 and S10).

With Sp in the minor groove conformation, the B-ring is positioned in the groove, but the A-ring protrudes into the helix and is stacked with adjacent bases. However, stacking of the Sp partner is disturbed, and this effect radiates beyond the immediate neighbors (Figures 2 and S9). The helix bends into the major groove to accommodate the B-ring in the minor groove, which therefore widens (Figures S4−S8). Again, there is perturbation to adjacent base pairs, which does not differ much in directionality in the various simulations, and is less pronounced than for the other conformational families with Sp(*anti*) (Figures 2 and S9). In this conformational family, hydrogen bonding between Sp and its partner base is found in the following cases: *R*-Sp·G(*anti*) pair (O5 of Sp to N2H2 of G) and *S*-Sp·G(*anti*) pair (O6 of Sp to N2H2 of G) (Figure S10).

Thermodynamic Analyses

Major Groove Conformers. We carried out thermodynamic analyses of our simulated structures (Table S6 (Supporting Information)), employing the MM-PBSA method (*72*) based on the ensemble of structures derived from the molecular dynamics simulations (see Methods). Thermodynamic and

structural analyses provide complementary information. As shown in Table 1, our thermodynamic analyses indicate that the duplexes containing the Sp residues have low energy structures with the Sp residing in the B-DNA major groove regardless of sequence and stereochemistry, except for *R*-Sp(*anti*)·T(*anti*). The low energy major groove conformation is mainly achieved by a rotation of the Sp glycosidic torsion angle to the *syn* domain. However, in the *R*-Sp·G pair, a low energy major groove position is achieved with the Sp(*anti*). Two hydrogen bonds between the Sp and the G are likely responsible for stabilizing this Sp(*anti*) structure (Figure 3). In addition, three low energy minor groove positions are found, namely, the *R*-Sp(*anti*)·A(*anti*) pair, and *R*- and *S*-Sp(*anti*)·T(*anti*) pairs. These Sp structures appear to be stabilized through hydrogen bonding and stacking. In the *R*-Sp(*anti*)·A(*anti*) case, the Sp forms three hydrogen bonds with adjacent bases (Table S5). In both the *R* and *S* Sp(*anti*)·T(*anti*) cases, the partner base T stacks well into the duplex due to hydrogen bonds between Sp and the T partner: *R*-Sp(*anti*)·T(*anti*), N2H2 of Sp to O2 of T (occupancy 41.0%); *S*-Sp(*anti*)·T(*anti*), bifurcated O5 and O6 of Sp to N3H3 of T (total occupancy 25.5%). The highest relative free energies are found for the most distorted intercalated structures, while the lowest relative free energies are all associated with less perturbed major and minor groove conformers.

Lower Energy R Stereoisomers. Our free energy analyses show that, in terms of absolute free energies, the *R* stereoisomers are somewhat lower in energy than the *S*, irrespective of the specific conformation and regardless of the partner base (Table S6). The differential stereochemistry of the stereoisomer pair in double stranded DNA appears to explain this effect. We note that the *R* stereoisomer has better hydrogen bonding to adjacent regions of the DNA, that there is less disturbance to the Watson−Crick base pairing adjacent to the lesion (Figure 4), and that there are better stacking interactions. Essentially, the opposite orientations of the *R* and *S* stereoisomers in the right-handed B-DNA helix position the perpendicular ring systems so that they differentially destabilize the double helix.

To illustrate this effect we consider the lowest energy structures in Table 1. For the Sp(*syn*) conformation structures, in which the Sp is in the major groove, the O6 atom of the *R*-Sp B-ring is 3′-oriented, while the *S*-Sp B-ring is 5′-oriented. We see from Figure 2 that the 5′ direction is more crowded in the right-hand-twisted B-DNA double helix. Accommodation of the Sp O6 atom of the *S* stereoisomer in this direction requires the Sp and the DNA to make adjustments that are more destabilizing. Thus, base stacking is adversely impacted, because the C5 residue must move to accommodate the O6 atom on the *S*-Sp B-ring, and therefore it stacks poorly with its 5′ neighboring base. Furthermore, the Sp A-ring stacks poorly with C7 and not at all with C5. The 3′-side neighboring C7·G16 Watson−Crick base pair is significantly perturbed (Figure 4), due to the 3′-orientation of the Sp A-ring. For the *R* stereoisomer, however, the O6 atom is 3′-directed in a less crowded situation in the groove, and has less destabilizing effects. Thus, base stacking is better on both sides, the Sp A-ring can stack with adjacent bases, perturbation of the 5′-side neighboring C5·G18 Watson−Crick base pair is lower, and more and better hydrogen bonds to the base partner and adjacent bases are possible than for the *S* stereoisomer (Figures 3 and S10 and Table S5).

For Sp in the *anti* conformation, there are four structures which contribute to their respective population mix, namely, the *R*-Sp(*anti*)·G(*syn*) pair, the *R*-Sp(*anti*)·A(*anti*) pair, and *R*- and *S*-Sp(*anti*)·T(*anti*) pairs. In these four cases, the Sp *R* stereoisomer is also lower in energy than the *S*. For the *R*-Sp(*anti*)·G(*syn*) pair, a major groove conformation, there are two hydrogen bonds between Sp and the partner, and an additional hydrogen bond between Sp and its 3′ base neighbor. However, for the *S* stereoisomer there is only one bifurcated hydrogen bond to the partner (Table S5). Furthermore, the structural analyses reveal that the duplex in the case of the *R* stereoisomer is less distorted than that of the *S*, with less distorted grooves and better stacking between the Sp B-ring and adjacent bases (Figures 2 and S9). For the *R*-Sp(*anti*)·A(*anti*) pair, a minor groove conformation, there is one hydrogen bond to its partner and there are two more to base neighbors, while in the *S* case there is only one hydrogen bond to the partner. The O6 of the *R*-Sp lesion is 5′-directed in the minor groove which is the less crowded direction and allows for a better accommodation of the lesion, as discussed above for the *syn* conformers, in which O6 is 3′-directed. In comparing the *R* and *S* Sp paired with T(*anti*), we find that the *R* stereoisomer DNA duplex is less bent (Figure S7), and the Sp participates in one more hydrogen bond (Table S5).

Stacking Interactions

A partial energetic assessment of stacking interactions can be obtained from van der Waals interactions between base pairs (or the Sp residue and partner with each adjacent base pair). These values are given in Table 2, Table S7 (Supporting Information), and Figure S22 (Supporting Information); they show that all modified duplexes have higher summed van der Waals interactions than the unmodified control. The differences are in the range of ∼2−11 kcal/mol depending on stereochemistry, partner, and conformation. While these values provide just one important energetic component contributing to stacking stabilization, the results show uniformly that the modified duplexes are less stabilized by stacking than the unmodified one.

Table 2: Sum of van der Waals Interaction Energies E_{vdW}[a]

	E_{vdW} (kcal/mol)		E_{vdW} (kcal/mol)
unmodified control	−121.6	*R*-Sp(*syn*)·G(*anti*)	−119.7
R-Sp(*syn*)·A(*anti*)	−117.3	*S*-Sp(*syn*)·G(*anti*)	−118.3
S-Sp(*syn*)·A(*anti*)	−118.3	*R*-Sp(*anti*)·G(*syn*)	−118.5
R-Sp(*anti*)·A(*anti*)	−112.3	*S*-Sp(*syn*)·T(*anti*)	−118.1
R-Sp(*syn*)·C(*anti*)	−114.0	*R*-Sp(*anti*)·T(*anti*)	−110.2
S-Sp(*syn*)·C(*anti*)	−113.3	*S*-Sp(*anti*)·T(*anti*)	−112.8

[a] The sum is over all pairs in the given duplex for the energetically favored modified duplexes (Table 1 and Figure 2) and the unmodified control. The two base pairs at the ends of the duplex are not included.

DISCUSSION

Duplex Destabilizing Sp Lesions. Our computed structural and thermodynamic studies have revealed that the Sp *R* and *S* stereoisomers in DNA duplexes energetically favor positioning in the B-DNA major groove; minor groove conformers are also low energy in some cases, depending on the

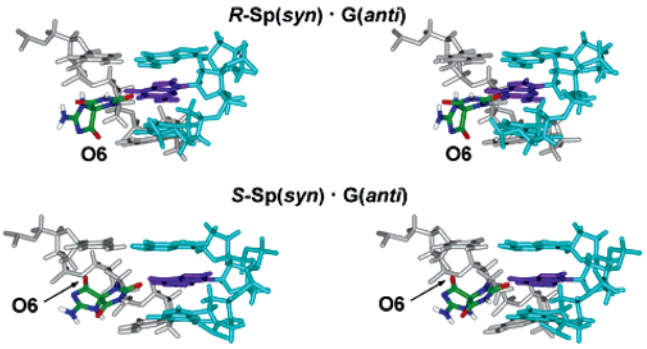

FIGURE 5: Stereoviews of the central 3-mer of Sp(*syn*)·G(*anti*) in stick models showing the opposite orientation of the O6 atoms. The Sp stereoisomers are colored by atom. The Sp partner G is in purple.

partner base. In most cases, the major groove positioning is favorably achieved by rotation of the Sp glycosidic bond to the *syn* domain. In addition, in one case, namely, the *R*-Sp(*anti*)·G(*syn*) pair, a low energy major groove Sp position was found with the Sp glycosidic bond *anti*. Also, three low energy cases occurred with Sp in the minor groove, namely, the *R*-Sp(*anti*)·A(*anti*) pair and *R*- and *S*-Sp(*anti*)·T(*anti*) pairs. Thus the chemical nature of the partner bases has an important influence on the structural preferences, due to their unique hydrogen bonding features. Full intercalation of the propeller-like Sp rings is severely distorting to the DNA duplex in every case, and is never favored energetically. However, the major or minor groove positions of the Sp lesions also perturb the DNA duplexes. This is manifested in opening of the major or minor grooves, disturbance to the Watson−Crick hydrogen bonding quality in adjacent base pairs, and disturbed base stacking, and these perturbations radiate beyond the immediate lesion vicinity (Table S7, Figures 2, S9, and S22). In the case of the minor groove conformer, significant bending of the DNA duplex also occurs. These distorting features are consistent with notable destabilization of Sp modified duplexes as evidenced by marked reduction in thermal stabilities of the duplexes with Sp lesions as compared to unmodified duplexes (Crean, C., Shafirovich, V., and Geacintov, N. E., unpublished observations).

Opposite Orientations and Differential Stabilities of R and S Sp Stereoisomers. Structures of the *R* and *S* stereoisomers differ through an opposite orientation phenomenon. The predominant major groove/*syn* conformational family is the only one found for both *R* and *S* stereoisomers. In each case, the O6 atom in the Sp B-ring is directed 3′ along the modified strand in the case of the *R* stereoisomer, while this atom is 5′-directed in the case of the *S* stereoisomer (Figure 5). This directional effect causes perturbed Watson−Crick hydrogen bonding and base stacking in the direction opposite to that of the O6 in the B-ring. In each case, the perpendicular Sp A-ring is driven to a position which creates the directional disturbance.

Our thermodynamic analyses indicate that the *R* stereoisomer modified duplex is in every case somewhat lower in absolute free energy than the *S* modified duplex. The structural analyses suggest that the origin of this differential stability is tied to the opposite orientations of the two stereoisomers. In the predominant major groove/*syn* conformational family, the O6 atom of the Sp B-ring is located in a more crowded groove location on the 5′-side of the *S* stereoisomer, requiring greater disturbance to the B-DNA duplex than in the case of the *R* stereoisomer; in the latter case, the 3′-directed O6 atom is in a more open position of the groove due to the right-handed twist of the B-DNA double helix, and its accommodation requires less distortion (Figure 2). Superimposed on this overall effect are specific structural phenomena derived from the nature of the base partner. These predominantly involve differential hydrogen bonding capabilities both with the Sp and with adjacent bases by the partner.

Table 3: Sp·A and Sp·G Hydrogen Bonds[a]

total no. of H bonds	*R*-Sp	*S*-Sp
Sp·A	1	1
Sp·G	2 + 1 bifurcated	1 bifurcated

[a] Hydrogen bonds are summed over all energetically favored Sp·A and Sp·G duplexes (Table 1).

Implications for Base Pairing Infidelity and Repair. Experimental mutagenicity studies, both in vitro and in vivo, suggest that the Sp·A and Sp·G pairs are preferentially formed during replication (*35*, *36*). The mutagenicity studies do not reveal incorporation of C and T opposite either Sp stereoisomer (*35*, *36*). Our simulations reveal hydrogen bonding schemes and stacking features which together could contribute to the preferential incorporation of G and A opposite both stereoisomers. Specifically, the extent of hydrogen bonding (Table S5) between *R*- and *S*-Sp and partner base follows the order G > A ≈ C > T; average stacking stabilization between *R*- and *S*-Sp and partner with base pair neighbors follows the order G > A > C ≈ T (Table 2). Stereoisomer-dependent differences in A or G incorporation opposite Sp have been noted (*36*), although these studies could not distinguish the absolute configuration of the two stereoisomers. In these studies it was found that, in *E. coli*, among the lesions which are bypassed, 72% G → C (Sp·G pair) and 27% G → T (Sp·A pair) transversions occur, in the case of Sp1, and 57% G → C and 41% G → T transversions in the case of Sp2. Our simulations suggest that the Sp *R* configuration favors pairing with G more than the *S* stereoisomer, based on the hydrogen bonding analyses between Sp and different partner bases. As shown in Figure 3 and Table 3, there are a total of one bifurcated and two normal hydrogen bonds for the Sp *R* stereoisomer with the two low energy structures containing a partner G residue; however, there is only one hydrogen bond in the case of the two low energy structures containing a partner A residue. For the *S*-Sp stereoisomer, there is only one bifurcated hydrogen bond with the one low energy structure containing the partner G, and one hydrogen bond with the one low energy structure containing a partner A (Table 3). Of course, the mutagenicity data reflect a very complex combination of factors involving the impact of the lesion on the polymerase active site structure, of which hydrogen bonding between template and dNTP is only one component (*86*). A structural feature, found in both nucleoside studies (*34*) and the present work, is a tendency to adopt an unusual sugar pucker in the O4′-endo region. Our present studies showed that this facile capability for O4′-endo pucker plays a role in stabilizing both *R*- and *S*-Sp(*syn*)·A(*anti*) hydrogen bonds,

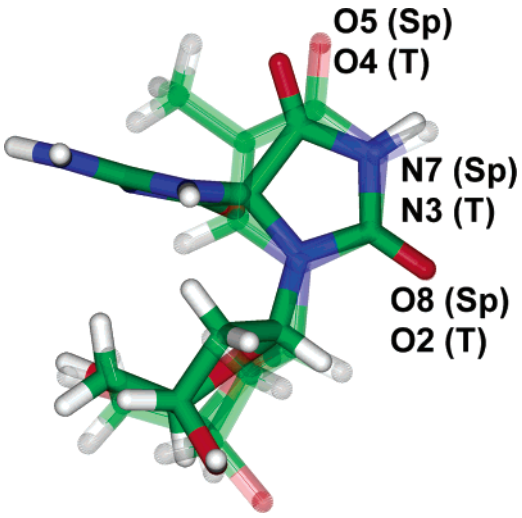

FIGURE 6: Overlap of *S*-Sp deoxyribonucleoside (*syn*) and thymine (T) deoxyribonucleoside (*anti*). The Sp's five-membered A-ring and T's six-membered ring are overlapped at atoms O8 (Sp) and O2 (T). Atom numbers are marked for Sp and T, respectively. Overlap of Sp A-ring with T is the same for the *R* stereoisomer. Molecules are colored by atom. The thymine deoxyribonucleoside is transparent.

and so might contribute to the observed G → T transversion mutations.

A notable feature of the Sp chemical structures is that the A-ring, irrespective of *R* and *S* stereochemistry, is a "pseudo-thymine" in its hydrogen bonding donor−acceptor properties and its single ring nature (Figure 6). When the largely favored *syn* conformation is adopted, this ring's thymine-like hydrogen bonding substituents are directed toward the helix interior. Pairing with a partner purine is therefore less strain on the DNA duplex than Sp(*syn*)·pyrimidine, which mimics a pyrimidine·pyrimidine pair. This may contribute to the absence of Sp·C and Sp·T pairing in the experimental mutagenicity studies.

The opposite orientations of the *R* and *S* configurations observed in our simulations could suggest differential treatment of the two lesions by repair enzymes. Our finding that the *S* stereoisomer duplex is less stable than the *R* stereoisomer might indicate a greater repair susceptibility for the *S* case, since the repair enzyme may sense and flip out (*87*) a less stable damaged nucleoside more readily. In addition, our prior computational studies on the nucleoside level suggested impeded rotation between *syn* and *anti* glycosidic bond orientations at the level of Sp nucleoside lesions (*34*). This could also impact lesion repair since it is possible that glycosylases may at times act on the *syn* form of Sp (*88*−*90*). Our duplex simulations in the present work did not reveal any *syn*/*anti* transition at the Sp lesions. However, hydrogen bonds between Sp and the partner bases evolved during the simulations, which also impeded such a transition; therefore the effect of the rotation behavior per se could not be evaluated from the duplex simulations.

We note that the free energy calculations are, of course, limited by the problem of sampling sufficiency in molecular dynamics simulations, together with issues relating to force field quality, which are ongoing frontier problems. Nonetheless, the ensembles of structures derived from MD trajectories can be acquired only by simulation and are proving valuable in elucidating structure−function relationships (*91*).

Our present study was carried out for the amino tautomer which is more stable according to QM calculations (*34*). This tautomer appears to be preferred as it has the advantage of permitting conjugation between the amino and carbonyl groups in the same ring. However, other tautomers might be possible. If experimental evidence indicating that other tautomers are important emerges in the future, it will provide impetus for further studies on a computational level.

CONCLUSION

Structural and thermodynamic studies employing molecular dynamics simulations show a favored conformation of Sp *R* and *S* stereoisomers in the major groove of the B-DNA duplex, regardless of the absolute configuration. Three cases of energetically favorable minor groove positions are also noted, but intercalation structures are disfavored for these propeller-like Sp structures. The lesions cause duplex distortion in the form of perturbation to neighboring Watson−Crick pairing and base stacking, as well as groove widening. Opposite orientations with respect to the 5′ to 3′ direction of the modified strand are found in the case of the *R* and *S* stereoisomers, and these opposite orientations produce different directional effects on the modified duplex. The chemical nature of the partner base determines specific hydrogen bonding and stacking properties of the damaged duplexes. These structural features can provide insights with respect to the mutagenic properties and susceptibilities to repair of these unusual base modifications, and suggest the possibility of stereochemical effects on their biochemical properties.

ACKNOWLEDGMENT

Computations were carried out on our cluster of Silicon Graphic Origin and Altix supercomputers and Octane workstations, as well as at the NYU Information Technology Services Origin supercomputer.

NOTE ADDED AFTER ASAP PUBLICATION

Figure 6 of this article, published on the Web on 9/16/05, has been replaced due to a minor error in the prior version. The correct version was posted on 9/23/05.

SUPPORTING INFORMATION AVAILABLE

Figure S1 shows representative starting models for the MD simulations. Figure S2 shows RMSD vs time plot of each molecular dynamics simulation. Figure S3 shows stereoviews of unmodified control trajectory-average structures of selected molecular dynamics simulation window. Figures S4−S8 show stereoviews of the trajectory-average structures and structural analyses data. Figure S9 shows stereoviews of the central 5-mer of the Sp trajectory-average duplex structures in CPK models. Figure S10 shows hydrogen bonds between Sp and partner base of high energy structures. Figure S11 shows the sums of the hydrogen bond occupancies of Sp neighboring Watson−Crick base pairs. Figures S12−S21 show trajectory average plots of duplex backbone torsion angles. Figure S22 shows van der Waals interaction energy vs base pair step. Table S1 shows glycosidic torsion χ values of Sp employed in duplex starting models. Table S2 shows added force field parameters for Sp lesions. Table S3 shows

AMBER atom type, connection type, and partial charge assignments for the Sp. Table S4 shows box sizes and numbers of waters in MD simulation starting models. Table S5 shows hydrogen bonds and occupancies involving Sp. Table S6 shows MM-PBSA free energy analysis components for each DNA duplex. Table S7 shows van der Waals interaction energies of adjacent base pairs and their sum over all pairs in the given duplex. This material is available free of charge via the Internet at http://pubs.acs.org.

REFERENCES

1. Epe, B. (1996) DNA damage profiles induced by oxidizing agents, *Rev. Physiol. Biochem. Pharmacol. 127*, 223−249.
2. Dizdaroglu, M. (1991) Chemical determination of free radical-induced damage to DNA, *Free Radical Biol. Med. 10*, 225−242.
3. Demple, B., and Harrison, L. (1994) Repair of oxidative damage to DNA: enzymology and biology, *Annu. Rev. Biochem. 63*, 915−948.
4. Cadet, J., Berger, M., Douki, T., and Ravanat, J. L. (1997) Oxidative damage to DNA: formation, measurement, and biological significance, *Rev. Physiol. Biochem. Pharmacol. 131*, 1−87.
5. Misiaszek, R., Crean, C., Joffe, A., Geacintov, N. E., and Shafirovich, V. (2004) Oxidative DNA damage associated with combination of guanine and superoxide radicals and repair mechanisms via radical trapping, *J. Biol. Chem. 279*, 32106−32115.
6. Lindahl, T. (1993) Instability and decay of the primary structure of DNA, *Nature 362*, 709−715.
7. Boiteux, S., and Radicella, J. P. (1999) Base excision repair of 8-hydroxyguanine protects DNA from endogenous oxidative stress, *Biochimie 81*, 59−67.
8. Fujikawa, K., Kamiya, H., and Kasai, H. (1998) The mutations induced by oxidatively damaged nucleotides, 5-formyl-dUTP and 5-hydroxy-dCTP, in Escherichia coli, *Nucleic Acids Res. 26*, 4582−4587.
9. Brajter-Toth, A., Goyal, R. N., Wrona, M. Z., Lacava, T., Nguyen, N. T., Dryhurst, G. (1981) Electrochemical and enzymic oxidation of biological purines, *Bioelectrochem. Bioenerg. 8*, 413−435.
10. Tretyakova, N. Y., Niles, J. C., Burney, S., Wishnok, J. S., and Tannenbaum, S. R. (1999) Peroxynitrite-induced reactions of synthetic oligonucleotides containing 8-oxoguanine, *Chem. Res. Toxicol. 12*, 459−466.
11. Niles, J. C., Wishnok, J. S., and Tannenbaum, S. R. (2001) A novel nitroimidazole compound formed during the reaction of peroxynitrite with 2′,3′,5′-tri-O-acetyl-guanosine, *J. Am. Chem. Soc. 123*, 12147−12151.
12. Henderson, P. T., Delaney, J. C., Gu, F., Tannenbaum, S. R., and Essigmann, J. M. (2002) Oxidation of 7,8-dihydro-8-oxoguanine affords lesions that are potent sources of replication errors in vivo, *Biochemistry 41*, 914−921.
13. Henderson, P. T., Neeley, W. L., Delaney, J. C., Gu, F., Niles, J. C., Hah, S. S., Tannenbaum, S. R., and Essigmann, J. M. (2005) Urea Lesion Formation in DNA as a Consequence of 7,8-Dihydro-8-oxoguanine Oxidation and Hydrolysis Provides a Potent Source of Point Mutations, *Chem. Res. Toxicol. 18*, 12−18.
14. Neeley, W. L., Delaney, J. C., Henderson, P. T., and Essigmann, J. M. (2004) In vivo bypass efficiencies and mutational signatures of the guanine oxidation products 2-aminoimidazolone and 5-guanidino-4-nitroimidazole, *J. Biol. Chem. 279*, 43568−43573.
15. Niles, J. C., Wishnok, J. S., and Tannenbaum, S. R. (2001) Spiroiminodihydantoin is the major product of the 8-oxo-7,8-dihydroguanosine reaction with peroxynitrite in the presence of thiols and guanosine photooxidation by methylene blue, *Org. Lett. 3*, 963−966.
16. Luo, W., Muller, J. G., Rachlin, E. M., and Burrows, C. J. (2000) Characterization of spiroiminodihydantoin as a product of one-electron oxidation of 8-Oxo-7,8-dihydroguanosine, *Org. Lett. 2*, 613−616.
17. Luo, W., Muller, J. G., and Burrows, C. J. (2001) The pH-dependent role of superoxide in riboflavin-catalyzed photooxidation of 8-oxo-7,8-dihydroguanosine, *Org. Lett. 3*, 2801−2804.
18. Luo, W., Muller, J. G., Rachlin, E. M., and Burrows, C. J. (2001) Characterization of hydantoin products from one-electron oxidation of 8-oxo-7,8-dihydroguanosine in a nucleoside model, *Chem. Res. Toxicol. 14*, 927−938.
19. Adam, W., Arnold, M. A., Grune, M., Nau, W. M., Pischel, U., and Saha-Moller, C. R. (2002) Spiroiminodihydantoin is a major product in the photooxidation of 2′-deoxyguanosine by the triplet states and oxyl radicals generated from hydroxyacetophenone photolysis and dioxetane thermolysis, *Org. Lett. 4*, 537−540.
20. Sugden, K. D., Campo, C. K., and Martin, B. D. (2001) Direct oxidation of guanine and 7,8-dihydro-8-oxoguanine in DNA by a high-valent chromium complex: a possible mechanism for chromate genotoxicity, *Chem. Res. Toxicol. 14*, 1315−1322.
21. Suzuki, T., Masuda, M., Friesen, M. D., and Ohshima, H. (2001) Formation of spiroiminodihydantoin nucleoside by reaction of 8-oxo-7,8-dihydro-2′-deoxyguanosine with hypochlorous acid or a myeloperoxidase-H(2)O(2)-Cl(-) system, *Chem. Res. Toxicol. 14*, 1163−1169.
22. Suzuki, T., and Ohshima, H. (2002) Nicotine-modulated formation of spiroiminodihydantoin nucleoside via 8-oxo-7,8-dihydro-2′-deoxyguanosine in 2′-deoxyguanosine-hypochlorous acid reaction, *FEBS Lett. 516*, 67−70.
23. Joffe, A., Geacintov, N. E., and Shafirovich, V. (2003) DNA Lesions Derived from the Site Selective Oxidation of Guanine by Carbonate Radical Anions, *Chem. Res. Toxicol. 16*, 1528−1538.
24. Hosford, M. E., Muller, J. G., and Burrows, C. J. (2004) Spermine participates in oxidative damage of guanosine and 8-oxoguanosine leading to deoxyribosylurea formation, *J. Am. Chem. Soc. 126*, 9540−9541.
25. Martinez, G. R., Medeiros, M. H., Ravanat, J. L., Cadet, J., and Di Mascio, P. (2002) [18O]-labeled singlet oxygen as a tool for mechanistic studies of 8-oxo-7,8-dihydroguanine oxidative damage: detection of spiroiminodihydantoin, imidazolone and oxazolone derivatives, *Biol. Chem. 383*, 607−617.
26. McCallum, J. E., Kuniyoshi, C. Y., and Foote, C. S. (2004) Characterization of 5-hydroxy-8-oxo-7,8-dihydroguanosine in the photosensitized oxidation of 8-oxo-7,8-dihydroguanosine and its rearrangement to spiroiminodihydantoin, *J. Am. Chem. Soc. 126*, 16777−16782.
27. Niles, J. C., Wishnok, J. S., and Tannenbaum, S. R. (2004) Spiroiminodihydantoin and guanidinohydantoin are the dominant products of 8-oxoguanosine oxidation at low fluxes of peroxynitrite: mechanistic studies with ^{18}O, *Chem. Res. Toxicol. 17*, 1510−1519.
28. Suzuki, T., Nakano, T., Masuda, M., and Ohshima, H. (2004) Epigallocatechin gallate markedly enhances formation of 8-oxo-7,8-dihydro-2′-deoxyguanosine in the reaction of 2′-deoxyguanosine with hypochlorous acid, *Free Radical Biol. Med. 36*, 1087−1093.
29. Ye, Y., Muller, J. G., Luo, W., Mayne, C. L., Shallop, A. J., Jones, R. A., and Burrows, C. J. (2003) Formation of ^{13}C-, ^{15}N-, and ^{18}O-labeled guanidinohydantoin from guanosine oxidation with singlet oxygen. Implications for structure and mechanism, *J. Am. Chem. Soc. 125*, 13926−13927.
30. Misiaszek, R., Uvaydov, Y., Crean, C., Geacintov, N. E., and Shafirovich, V. (2005) Combination reactions of superoxide with 8-Oxo-7,8-dihydroguanine radicals in DNA: kinetics and end products, *J. Biol. Chem. 280*, 6293−6300.
31. Misiaszek, R., Crean, C., Geacintov, N. E., and Shafirovich, V. (2005) Combination of nitrogen dioxide radicals with 8-oxo-7,8-dihydroguanine and guanine radicals in DNA: oxidation and nitration end-products, *J. Am. Chem. Soc. 127*, 2191−2200.
32. Slade, P. G., Hailer, M. K., Martin, B. D., and Sugden, K. D. (2005) Guanine-Specific Oxidation of Double-Stranded DNA by Cr(VI) and Ascorbic Acid Forms Spiroiminodihydantoin and 8-Oxo-2′-deoxyguanosine., *Chem. Res. Toxicol. 18*, 1140−1149.
33. Hailer, M. K., Slade, P. G., Martin, B. D., and Sugden, K. D. (2005) Nei deficient *Escherichia coli* are sensitive to chromate and accumulate the oxidized guanine lesion spiroiminodihydantoin, *Chem. Res. Toxicol.* Web release date Aug 12, 2005.
34. Jia, L., Shafirovich, V., Shapiro, R., Geacintov, N. E., and Broyde, S. (2005) Spiroiminodihydantoin Lesions Derived from Guanine Oxidation: Structures, Energetics, and Functional Implications, *Biochemistry 44*, 6043−6051.
35. Kornyushyna, O., Berges, A. M., Muller, J. G., and Burrows, C. J. (2002) In vitro nucleotide misinsertion opposite the oxidized guanosine lesions spiroiminodihydantoin and guanidinohydantoin and DNA synthesis past the lesions using Escherichia coli DNA polymerase I (Klenow fragment), *Biochemistry 41*, 15304−15314.
36. Henderson, P. T., Delaney, J. C., Muller, J. G., Neeley, W. L., Tannenbaum, S. R., Burrows, C. J., and Essigmann, J. M. (2003) The hydantoin lesions formed from oxidation of 7,8-dihydro-8-

oxoguanine are potent sources of replication errors in vivo, *Biochemistry 42*, 9257−9262.
37. Hailer, M. K., Slade, P. G., Martin, B. D., Rosenquist, T. A., and Sugden, K. D. (2005) Recognition of the oxidized lesions spiroiminodihydantoin and guanidinohydantoin in DNA by the mammalian base excision repair glycosylases NEIL1 and NEIL2, *DNA Repair 4*, 41−50.
38. Michaels, M. L., Cruz, C., Grollman, A. P., and Miller, J. H. (1992) Evidence that MutY and MutM combine to prevent mutations by an oxidatively damaged form of guanine in DNA, *Proc. Natl. Acad. Sci. U.S.A. 89*, 7022−7025.
39. Michaels, M. L., Tchou, J., Grollman, A. P., and Miller, J. H. (1992) A repair system for 8-oxo-7,8-dihydrodeoxyguanine, *Biochemistry 31*, 10964−10968.
40. David, S. S., and Williams, S. D. (1998) Chemistry of Glycosylases and Endonucleases Involved in Base-Excision Repair, *Chem. Rev. 98*, 1221−1262.
41. Leipold, M. D., Muller, J. G., Burrows, C. J., and David, S. S. (2000) Removal of hydantoin products of 8-oxoguanine oxidation by the Escherichia coli DNA repair enzyme, FPG, *Biochemistry 39*, 14984−14992.
42. Hazra, T. K., Muller, J. G., Manuel, R. C., Burrows, C. J., Lloyd, R. S., and Mitra, S. (2001) Repair of hydantoins, one electron oxidation product of 8-oxoguanine, by DNA glycosylases of Escherichia coli, *Nucleic Acids Res. 29*, 1967−1974.
43. Leipold, M. D., Workman, H., Muller, J. G., Burrows, C. J., and David, S. S. (2003) Recognition and removal of oxidized guanines in duplex DNA by the base excision repair enzymes hOGG1, yOGG1, and yOGG2, *Biochemistry 42*, 11373−11381.
44. Weinberg, R. A. (1996) How cancer arises, *Sci. Am. 275*, 62−70.
45. Vineis, P., Malats, N., Porta, M., and Real, F. X. (1999) Human cancer, carcinogenic exposures and mutation spectra, *Mutat. Res. 436*, 185−194.
46. Fisher, D. E. (2001) The p53 tumor suppressor: critical regulator of life & death in cancer, *Apoptosis 6*, 7−15.
47. Greenberg, M. M. (2004) In vitro and in vivo effects of oxidative damage to deoxyguanosine, *Biochem. Soc. Trans. 32*, 46−50.
48. Hingerty, B. E., Figueroa, S., Hayden, T. L., and Broyde, S. (1989) Prediction of DNA-Structure from Sequence—a Buildup Technique, *Biopolymers 28*, 1195−1222.
49. Brown, T., Hunter, W. N., Kneale, G., and Kennard, O. (1986) Molecular structure of the G.A base pair in DNA and its implications for the mechanism of transversion mutations, *Proc. Natl. Acad. Sci. U.S.A. 83*, 2402−2406.
50. Lane, A. N., and Peck, B. (1995) Conformational flexibility in DNA duplexes containing single G.G mismatches, *Eur. J. Biochem. 230*, 1073−1087.
51. Berman, H. M., Olson, W. K., Beveridge, D. L., Westbrook, J., Gelbin, A., Demeny, T., Hsieh, S. H., Srinivasan, A. R., and Schneider, B. (1992) The nucleic acid database. A comprehensive relational database of three-dimensional structures of nucleic acids, *Biophys. J. 63*, 751−759.
52. Case, D. A., Darden, T. A., Cheatham, T. E., III, Simmerling, C. L., Wang, J., Duke, R. E., Luo, R., Merz, K. M., Wang, B., Pearlman, D. A., Crowley, M., Brozell, S., Tsui, V., Gohlke, H., Mongan, J., Hornak, V., Cui, G., Beroza, P., Schafmeister, C., Caldwell, J. W., Ross, W. S., and Kollman, P. A. (2004) AMBER 8.0, University of California, San Francisco.
53. Cornell, W. D., Cieplak, P., Bayly, C. I., Gould, I. R., Merz, K. M., Ferguson, D. M., Spellmeyer, D. C., Fox, T., Caldwell, J. W., and Kollman, P. A. (1995) A Second Generation Force Field for the Simulation of Proteins, Nucleic Acids, and Organic Molecules, *J. Am. Chem. Soc. 117*, 5179−5197.
54. Wang, J. M., Cieplak, P., and Kollman, P. A. (2000) How well does a restrained electrostatic potential (RESP) model perform in calculating conformational energies of organic and biological molecules?, *J. Comput. Chem. 21*, 1049−1074.
55. Cieplak, P., Cornell, W. D., Bayly, C., and Kollman, P. A. (1995) Application of the Multimolecule and Multiconformational Resp Methodology to Biopolymers—Charge Derivation for DNA, RNA, and Proteins, *J. Comput. Chem. 16*, 1357−1377.
56. Hehre, W. J., Ditchfie, R., and Pople, J. A. (1972) Self-Consistent Molecular-Orbital Methods. 12. Further Extensions of Gaussian-Type Basis Sets for Use in Molecular-Orbital Studies of Organic-Molecules, *J. Chem. Phys. 56*, 2257−2261.
57. Frisch, M. J., Trucks, G. W., Schlegel, H. B., Scuseria, G. E., Robb, M. A., Cheeseman, J. R., Zakrzewski, V. G., Montgomery, J. A., Jr., Stratmann, R. E., Burant, J. C., Dapprich, S., Millam, J. M., Daniels, A. D., Kudin, K. N., Strain, M. C., Farkas, O., Tomasi, J., Barone, V., Cossi, M., Cammi, R., Mennucci, B., Pomelli, C., Adamo, C., Clifford, S., Ochterski, J., Petersson, G. A., Ayala, P. Y., Cui, Q., Morokuma, K., Malick, D. K., Rabuck, A. D., Raghavachari, K., Foresman, J. B., Cioslowski, J., Ortiz, J. V., Baboul, A. G., Stefanov, B. B., Liu, G., Liashenko, A., Piskorz, P., Komaromi, I., Gomperts, R., Martin, R. L., Fox, D. J., Keith, T., Al-Laham, M. A., Peng, C. Y., Nanayakkara, A., Gonzalez, C., Challacombe, M., Gill, P. M. W., Johnson, B. G., Chen, W., Wong, M. W., Andres, J. L., Head-Gordon, M., Replogle, E. S., and Pople, J. A. (1998) *Gaussian 98*, revision A.7, Gaussian, Inc., Pittsburgh, PA.
58. Bayly, C. I., Cieplak, P., Cornell, W., and Kollman, P. A. (1993) A well-behaved electrostatic potential based method using charge restraints for deriving atomic charges: the RESP model, *J. Phys. Chem. 97*, 10269−10280.
59. Ryckaert, J. P., Ciccotti, G., and Berendsen, H. J. C. (1977) Numerical-Integration of Cartesian Equations of Motion of a System with Constraints—Molecular-Dynamics of N-Alkanes, *J. Comput. Phys. 23*, 327−341.
60. Harvey, S. C., Tan, R. K. Z., and Cheatham, T. E. (1998) The flying ice cube: Velocity rescaling in molecular dynamics leads to violation of energy equipartition, *J. Comput. Chem. 19*, 726−740.
61. Darden, T., York, D., and Pedersen, L. (1993) Particle Mesh Ewald—an N.Log(N) Method for Ewald Sums in Large Systems, *J. Chem. Phys. 98*, 10089−10092.
62. Essmann, U., Perera, L., Berkowitz, M. L., Darden, T., Lee, H., and Pedersen, L. G. (1995) A Smooth Particle Mesh Ewald Method, *J. Chem. Phys. 103*, 8577−8593.
63. Jorgensen, W. L., Chandrasekhar, J., Madura, J. D., Impey, R. W., and Klein, M. L. (1983) Comparison of Simple Potential Functions for Simulating Liquid Water, *J. Chem. Phys. 79*, 926−935.
64. Berendsen, H. J. C., Postma, J. P. M., Vangunsteren, W. F., Dinola, A., and Haak, J. R. (1984) Molecular-Dynamics with Coupling to an External Bath, *J. Chem. Phys. 81*, 3684−3690.
65. Yan, S. X., Shapiro, R., Geacintov, N. E., and Broyde, S. (2001) Stereochemical, structural, and thermodynamic origins of stability differences between stereoisomeric benzo[a]pyrene diol epoxide deoxyadenosine adducts in a DNA mutational hot spot sequence, *J. Am. Chem. Soc. 123*, 7054−7066.
66. Altona, C., and Sundaralingam, M. (1972) Conformational analysis of the sugar ring in nucleosides and nucleotides. A new description using the concept of pseudorotation, *J. Am. Chem. Soc. 94*, 8205−8212.
67. Case, D. A., Pearlman, D. A., Caldwell, J. W., Cheatham, T. E., III, Wang, J., Ross, W. S., Simmerling, C. L., Darden, T. A., Merz, K. M., Stanton, R. V., Cheng, A. L., Vincent, J. J., Crowley, M., Tsui, V., Gohlke, H., Radmer, R. J., Duan, Y., Pitera, J., Massova, I., Seibel, G. L., Singh, U. C., Weiner, P. K., and Kollman, P. A. (2002) AMBER 7.0, University of California, San Francisco.
68. Saenger, W. (1984) *Principles of Nucleic Acid Structure*, Springer-Verlag, New York.
69. Ravishanker, G., Swaminathan, S., Beveridge, D. L., Lavery, R., and Sklenar, H. (1989) Conformational and helicoidal analysis of 30 PS of molecular dynamics on the d(CGCGAATTCGCG) double helix: "curves", dials and windows, *J. Biomol. Struct. Dyn. 6*, 669−699.
70. Ravishanker, G., Wang, W., and Beveridge, D. L. Molecular Dynamics Analysis Toolchest, Wesleyan University, Middletown, CT.
71. Lavery, R., and Sklenar, H. (1988) The Definition of Generalized Helicoidal Parameters and of Axis Curvature for Irregular Nucleic-Acids, *J. Biomol. Struct. Dyn. 6*, 63−91.
72. Kollman, P. A., Massova, I., Reyes, C., Kuhn, B., Huo, S., Chong, L., Lee, M., Lee, T., Duan, Y., Wang, W., Donini, O., Cieplak, P., Srinivasan, J., Case, D. A., and Cheatham, T. E., 3rd (2000) Calculating structures and free energies of complex molecules: combining molecular mechanics and continuum models, *Acc. Chem. Res. 33*, 889−897.
73. Wang, W., and Kollman, P. A. (2000) Free energy calculations on dimer stability of the HIV protease using molecular dynamics and a continuum solvent model, *J. Mol. Biol. 303*, 567−582.
74. Reyes, C. M., and Kollman, P. A. (2000) Investigating the binding specificity of U1A-RNA by computational mutagenesis, *J. Mol. Biol. 295*, 1−6.

75. Lee, M. R., Duan, Y., and Kollman, P. A. (2000) Use of MM-PB/SA in estimating the free energies of proteins: application to native, intermediates, and unfolded villin headpiece, *Proteins 39*, 309−316.
76. Wang, J., Morin, P., Wang, W., and Kollman, P. A. (2001) Use of MM-PBSA in reproducing the binding free energies to HIV-1 RT of TIBO derivatives and predicting the binding mode to HIV-1 RT of efavirenz by docking and MM-PBSA, *J. Am. Chem. Soc. 123*, 5221−5230.
77. Huo, S., Massova, I., and Kollman, P. A. (2002) Computational alanine scanning of the 1:1 human growth hormone-receptor complex, *J. Comput. Chem. 23*, 15−27.
78. Jayaram, B., McConnell, K. J., Dixit, S. B., and Beveridge, D. L. (1999) Free energy analysis of protein-DNA binding: The EcoRI endonuclease-DNA complex, *J. Comput. Phys. 151*, 333−357.
79. Yan, S., Wu, M., Buterin, T., Naegeli, H., Geacintov, N. E., and Broyde, S. (2003) Role of base sequence context in conformational equilibria and nucleotide excision repair of benzo[a]pyrene diol epoxide-adenine adducts, *Biochemistry 42*, 2339−2354.
80. Honig, B., and Nicholls, A. (1995) Classical Electrostatics in Biology and Chemistry, *Science 268*, 1144−1149.
81. Connolly, M. L. (1983) Analytical Molecular-Surface Calculation, *J. Appl. Crystallogr. 16*, 548−558.
82. Sitkoff, D., Sharp, K. A., and Honig, B. (1994) Accurate Calculation of Hydration Free-Energies Using Macroscopic Solvent Models, *J. Phys. Chem. 98*, 1978−1988.
83. Sanner, M. F., Olson, A. J., and Spehner, J. C. (1996) Reduced surface: an efficient way to compute molecular surfaces, *Biopolymers 38*, 305−320.
84. Srinivasan, J., Cheatham, T. E., Cieplak, P., Kollman, P. A., and Case, D. A. (1998) Continuum solvent studies of the stability of DNA, RNA, and phosphoramidate−DNA helices, *J. Am. Chem. Soc. 120*, 9401−9409.
85. Yan, S., Wu, M., Patel, D. J., Geacintov, N. E., and Broyde, S. (2003) Simulating structural and thermodynamic properties of carcinogen-damaged DNA, *Biophys. J. 84*, 2137−2148.
86. Kool, E. T. (2001) Hydrogen bonding, base stacking, and steric effects in DNA replication, *Annu. Rev. Biophys. Biomol. Struct. 30*, 1−22.
87. McCullough, A. K., Dodson, M. L., and Lloyd, R. S. (1999) Initiation of base excision repair: glycosylase mechanisms and structures, *Annu. Rev. Biochem. 68*, 255−285.
88. Fromme, J. C., and Verdine, G. L. (2003) DNA lesion recognition by the bacterial repair enzyme MutM, *J. Biol. Chem. 278*, 51543−51548.
89. Perlow-Poehnelt, R. A., Zharkov, D. O., Grollman, A. P., and Broyde, S. (2004) Substrate discrimination by formamidopyrimidine-DNA glycosylase: distinguishing interactions within the active site, *Biochemistry 43*, 16092−16105.
90. Amara, P., Serre, L., Castaing, B., and Thomas, A. (2004) Insights into the DNA repair process by the formamidopyrimidine-DNA glycosylase investigated by molecular dynamics, *Protein Sci. 13*, 2009−2021.
91. Cheatham, T. E., 3rd (2004) Simulation and modeling of nucleic acid structure, dynamics and interactions, *Curr. Opin. Struct. Biol. 14*, 360−367.

BI050790V